Electronic supplementary data

Phenoxo-bridged dinuclear mixed valence cobalt(III/II) complexes with reduced Schiff base ligands: Synthesis, characterization, band gap measurement and fabrication of Schottky barier diodes

Abhisek Banerjee,[a] Dhananjoy Das,[b] Partha Pratim Ray,[b] Snehasis Banerjee[c] and Shouvik Chattopadhyay,*

[a]*Department of Chemistry, Inorganic Section, Jadavpur University, Kolkata- 700032, India. E-mail: shouvik.chem@gmail.com*

[b]*Department of Physics, Jadavpur University, Kolkata-700032, India. E-mail: parthapray@yahoo.com*

[c]*Govt. College of Engineering and Leather Technology, Salt Lake Sector-III, Block- LB, Kolkata 700106, India*

Hirshfeld Surface Analysis

Hirshfeld surfaces[1-2] and the associated two-dimensional (2D)[3-5] plots were calculated using Crystal Explorer,[6] with bond lengths to hydrogen atoms set to standard values[7]. For each

point on the Hirshfeld isosurface, two distances, d_e (the distance from the point to the nearest nucleus external to the surface) and d_i (the distance to the nearest nucleus internal to the surface), are defined. The normalized contact distance (d_{norm}) based on d_e and d_i is given by

$$d_{norm} = \frac{(d_i - r_i^{vdw})}{r_i^{vwd}} + \frac{(d_e - r_e^{vdw})}{r_e^{vwd}}$$

where r_i^{vdW} and r_e^{vdW} are the van der Waals radii of the atoms. The value of d_{norm} is negative or positive depending on intermolecular contacts being shorter or longer than the van der Waals separations. The parameter d_{norm} displays a surface with a red−white−blue color scheme, where bright red spots highlight shorter contacts, white areas represent contacts around the van der Waals separation, and blue regions are devoid of close contacts. For a given crystal structure and set of spherical atomic electron densities, the Hirshfeld surface is unique[8] and thus it suggests the possibility of gaining additional insight into the intermolecular interaction of molecular crystals.

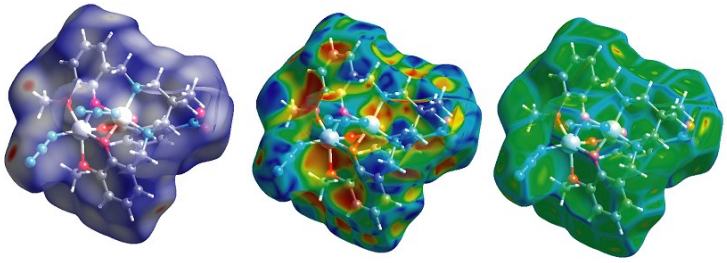

Complex 1

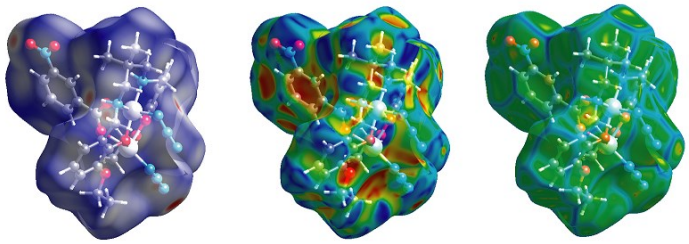

Complex 2

Figure S1: Hirshfeld surfaces mapped with d_{norm} (left column), shape index (middle) and curvedness (right column) of complexes **1** and **2**.

The Hirshfeld surfaces of both complexes have been mapped over d_{norm} (range -0.1 Å to 1.5 Å) shape index and curvedness (Figure S1). Two-dimensional fingerprint plots obtained from Hirshfeld surface analysis may also be useful in order to get quantitative information about the individual contribution of such supramolecular interactions in the crystal packing. Intermolecular interactions appear as distinct spikes in this plot. Complementary regions are observable in the two-dimensional fingerprint plots where one molecule act as donor ($d_e > d_i$) and the other as an acceptor ($d_e < d_i$). In the fingerprint plots (Figure S2), the most dominant interactions have been observed for N···H/H···N contacts {25.3% for complex **1** and 23.1% for complex **2** of the total Hirshfeld surface} and C···H/H···C contacts {19.0% for complex **1** and 20.0% for complex **2** of the total Hirshfeld surface} while contribution of interactions coming from O···H contacts are very comparatively less i.e. 17% and 14.3% for complexes **1** and **2** respectively.

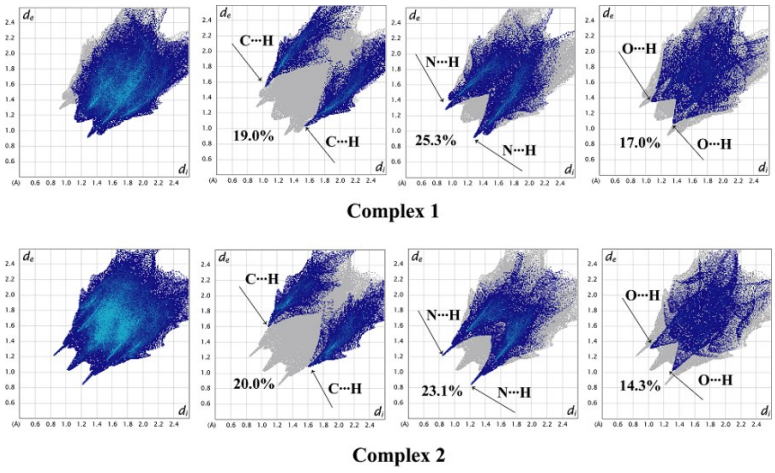

Figure S2: Fingerprint plot: Full (extreme left), resolved into H···C/C···H (second from the left), H···N/N···H (second from the right) and H···O/O···H (extreme right) contacts contributed to the total Hirshfeld Surface area of complexes **1** and **2**.

Table S1: Selected bond lengths (Å) of complexes **1** and **2**.

Complex	**1**	**2**
Co(1)-O(1)	1.946(2)	1.935(2)
Co(1)-O(2)	1.931(4)	1.943(3)
Co(1)-O(5)	1.944(4)	1.946(3)
Co(1)-N(1)	1.979(3)	1.971(3)
Co(1)-N(2)	1.988(3)	1.972(3)
Co(1)-N(3)	1.917(3)	1.910(3)
Co(2)-O(1)	2.034(3)	2.012(3)
Co(2)-O(2)	2.025(2)	2.024(2)
Co(2)-O(3)	2.292(3)	2.387(3)
Co(2)-O(4)	2.241(3)	2.345(3)
Co(2)-O(6)	2.063(3)	2.038(3)
Co(2)-N(4)	1.947(5)	1.947(5)

Table S2: Selected bond angles (°) of complexes **1** and **2**.

	1	**2**		**1**	**2**
O(1)-Co(1)-O(2)	79.23(10)	80.08(10)	O(1)-Co(2)-O(2)	75.04(9)	76.38(10)
O(1)-Co(1)-O(5)	92.25(11)	91.41(11)	O(1)-Co(2)-O(3)	75.46(12)	74.72(10)
O(1)-Co(1)-N(1)	92.71(13)	91.71(13)	O(1)-Co(2)-O(4)	150.28(11)	150.05(9)
O(1)-Co(1)-N(2)	171.48(12)	172.77(12)	O(1)-Co(2)-O(6)	92.11(11)	93.25(11)
O(1)-Co(1)-N(3)	92.54(14)	92.95(13)	O(1)-Co(2)-N(4)	114.80(2)	103.61(1)
O(2)-Co(1)-O(5)	93.99(10)	93.06(10)	O(2)-Co(2)-O(3)	149.11(11)	149.25(10)
O(2)-Co(1)-N(1)	171.94(12)	171.75(12)	O(2)-Co(2)-O(4)	75.84(10)	73.81(10)
O(2)-Co(1)-N(2)	92.28(11)	92.97(11)	O(2)-Co(2)-O(6)	92.50(11)	91.35(11)
O(2)-Co(1)-N(3)	91.84(11)	90.88(12)	O(2)-Co(2)-N(4)	116.03(16)	112.31(15)
O(5)-Co(1)-N(1)	86.20(13)	87.91(12)	O(3)-Co(2)-O(4)	131.75(13)	133.73(11)
O(5)-Co(1)-N(2)	87.60(11)	86.93(11)	O(3)-Co(2)-O(6)	79.62(11)	80.14(11)

O(5)-Co(1)-N(3)	173.06(13)	174.57(12)	O(3)-Co(2)-N(4)	84.80(15)	84.71(10)
N(1)-Co(1)-N(2)	95.75(13)	95.26(13)	O(4)-Co(2)-O(6)	83.36(11)	84.72(9)
N(1)-Co(1)-N(3)	88.57(13)	88.72(12)	O(4)-Co(2)-N(4)	83.52(4)	90.35(15)
N(2)-Co(1)-N(3)	88.40(14)	76.38(10)	O(6)-Co(2)-N(4)	144.34(4)	153.45(1)

Computational details

All calculations were performed with Gaussian 09. To know the exact position of hydrogen atoms of both molecules were optimized in their ground spin state using spin-unrestricted B3LYP density functional starting from their crystallographic geometries. Here, Los Alamos Effective Core Potentials lanL2DZ basis set was employed for the Fe atom. On the other hand, the split-valence 6-31G(d) basis set was applied for the other atoms.

The topological features derived from Bader's theory of atoms in molecules (AIM) approach was applied to understand the electron-density features like charge density (ρ) and Laplacian of charge density ($\nabla^2\rho$) using ADF2014.10. The recently developed Reduced Density Gradient (RDG) based NCI (non-covalent interactions) index calculations were applied for real-space visualization of both attractive (van der Waals and hydrogen-bonding) and repulsive (steric) interactions based on properties of the electron density. Herein, the single-point calculations were based on the structure obtained from X-ray studies and in these structures, the hydrogen atom positions were optimized before computation.

To calculate the hydrogen bond energy the following latest formula Emamian *et al*.[9] derived by at the very accurate CCSD(T)/jul-cc-pVTZ level including BSSE correction as well as SAPT2+(3)δMP2/aug-cc-pVTZ level, this allows the bond energy to be decomposed into

physically meaningful components to shed light on the electronic nature of the considered hydrogen bond interactions:

$$\text{Hydrogen bond energy (kcal/mol)} = -223.08 \times \rho_{BCP}(\text{a. u.}) + 0.7423$$

Physical measurements

Elemental analyses (carbon, hydrogen and nitrogen) were performed using a Perkin Elmer 240C elemental analyzer. IR spectra in KBr (4500-500 cm^{-1}) were recorded with a Perkin Elmer Spectrum Two spectrophotometer. Electronic spectra were recorded in acetonitrile medium at room temperature in the range 200-800 nm on a Perkin Elmer Lambda 35 UV-visible spectrophotometer. The magnetic susceptibility measurement was done with an EG & PAR vibrating sample magnetometer (Model 155) at room temperature and diamagnetic corrections were performed using Pascal's constants.[10] The electrospray ionization mass spectra were recorded using a Waters QTOF Micro YA263.

BVS calculation

The bond valence sum (BVS) calculations have been carried out to determine the oxidation state of cobalt centers, Co(1) and Co(2), in the titled complexes. The results are in good agreement for confirming the existence of mixed valence states of cobalt in these complexes. The deviation of the BVS values from an integer value may happen due to various reasons i.e. possible steric constraints, excessive thermal motion, problems with the crystal structure report or some combination of all of these effects.The BVS values calculated for Co(1) and Co(2) centers in complexes **1** and **2** have been listed in Table S1.

Table S3: BVS (Bond Valence Sum) values of the metal centres of complexes **1** and **2**:

Complex	**BVS of cobalt(III)**	**BVS of cobalt(II)**
1	3.06	2.08
2	3.09	2.04

IR and Electronic Spectra

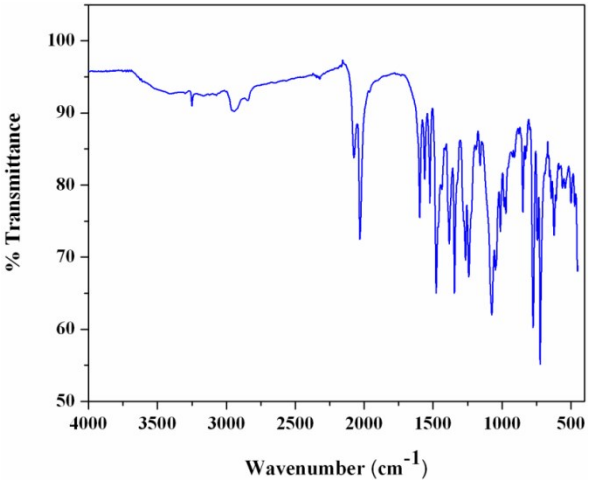

Figure S3: IR spectrum of complex **1**.

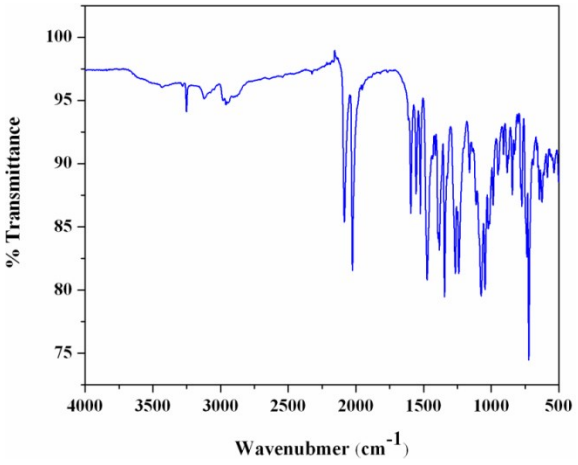

Figure S4: IR spectrum of complex **2**.

Table S4: Calculated energy absorption properties of H_2L^1 and H_2L^2 ligands by using the B3LYP/6-31G(d,p)method.

Wavelength (in nm)	Oscillator strength	Major contribution of FMOs
H_2L^1		
273	0.0018	HOMO->LUMO (45%), HOMO->L+1 (53%)
269	0.0037	HOMO->LUMO (53%), HOMO->L+1 (45%)
253	0.0583	H-2->LUMO (20%), H-1->LUMO (65%)
247	0.0152	H-1->L+1 (22%), HOMO->L+2 (23%), HOMO->L+3 (40%)
245	0.0381	H-1->L+1 (39%), HOMO->L+2 (20%), HOMO->L+3 (15%)
241	0.0005	H-2->LUMO (61%), H-1->LUMO (28%)
239	0.0025	HOMO->L+2 (55%), HOMO->L+3 (41%)
232	0.0004	H-2->L+1 (74%), H-1->L+1 (23%)
221	0.0359	H-1->L+2 (89%)
217	0.0073	H-2->L+2 (27%), H-1->L+3 (66%)
H_2L^2		
262	0.0008	HOMO->LUMO (48%), HOMO->L+1 (50%)
258	0.0046	HOMO->LUMO (51%), HOMO->L+1 (47%)
251	0.0587	H-2->LUMO (24%), H-1->LUMO (63%)
244	0.0547	H-1->L+1 (24%), HOMO->L+2 (24%), HOMO->L+3 (42%)
239	0.0027	H-1->L+1 (38%), HOMO->L+2 (22%), HOMO->L+3 (17%)
238	0.0005	H-2->LUMO (58%), H-1->LUMO (32%)

233	0.0013	HOMO->L+2 (56%), HOMO->L+3 (42%)
233	0.0005	H-2->L+1 (75%), H-1->L+1 (20%)
222	0.0356	H-1->L+2 (90%)
219	0.0073	H-2->L+2 (31%), H-1->L+3 (67%)

Optoelectronic properties

Device fabrication

To fabricate the Schottky diode, an ITO coated glass substrate was cleaned by using 2-propanol, acetone and distilled water sequentially and repeatedly. In parallel, we have made a well-dispersed medium of the synthesized complexes **1** and **2** in DMF (N, N-dimethylformamide) by ultra-sonicating for 2 hr. The as-prepared dispersed medium was coated onto the ITO coated glass substrate using the spin coating unit (SCU 2700) at the rate of 1200 rpm for 3 min. The as-prepared film was then dried in a vacuum oven. Finally, the aluminium electrode as metal contact was deposited using the Vacuum Coating Unit 12A4D of HINDHIVAC under pressure 10^{-6} Torr. The effective area of the Schottky contact deposited by shadow mask was measured as 7.065×10^{-6} m^{-2}.

To estimate the energy band gap, we used the Tauc's equation,[11] which is written as

$$(\alpha h\nu)^n = C(h\nu - E_g) \qquad \text{(S1)}$$

where α is the absorption coefficient, h is the Planck's constant, ν is the frequency of the light, C is an arbitrary constant, Eg is the optical band gap and n =2 and ½ is corresponding to the allowed direct and indirect electronic transitions.

Analysis of diode parameters

According to thermionic emission theory of Schottky diode, the current density of the fabricated diode can be expressed as,

$$J = J_0[e^{\frac{q_e V_0}{\eta k_B T}} - 1] \qquad \text{(S2)}$$

Where J_0 is the saturation current density, q_e is the electronic charge, V_0 is the voltage across the diode, η is the ideality factor, k_B is the Boltzmann constant and T is the absolute temperature. The saturation current density J_0 can be expressed as,[12]

$$J_0 = A^* T^2 e^{\frac{-q_e \phi_B}{k_B T}} \qquad \text{(S3)}$$

Where A^* is the effective Richardson constant and ϕ_B is the barrier height. Here, the effective diode area was measured as 7.065×10^{-6} m^2 and the effective Richardson constant was considered as $1.202 \times 10^6 Am^{-2}K^{-2}$.

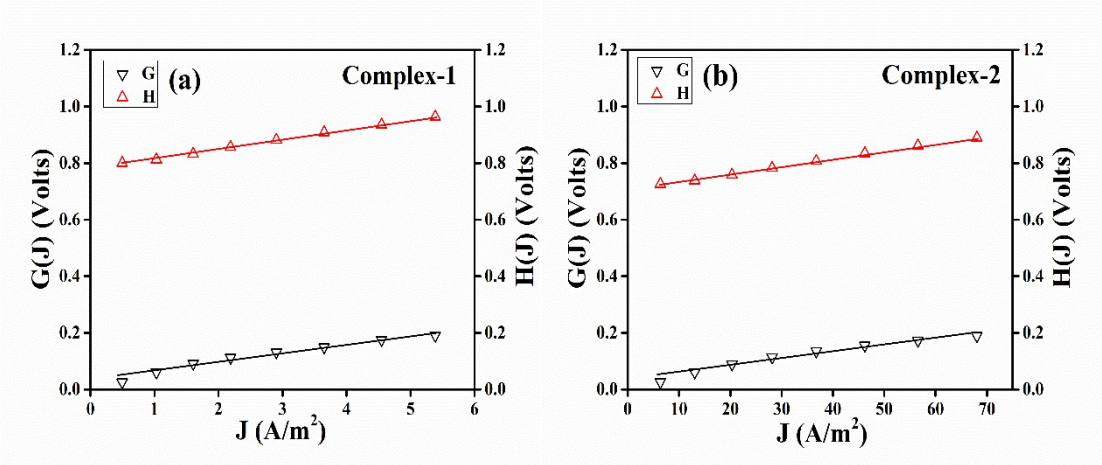

Figure S5: G(J) and H(J) vs. J plot for (a) complex **1** and (b) complex **2**.

Using equation (S2) and (S3), two linear equations (S4 and S5) were formed, which helped us to find out the values of ideality factor (η), barrier height (ϕ_B) and series resistance (R_S) of the Al/complex/ITO configured metal-semiconductor diode.[13]

$$G(J) = R_s A_{eff} J + \frac{\eta k_B T}{q_e} \qquad \text{(S4)}$$

$$H(J) = R_S A_{eff} J + \eta \phi_B \qquad \text{(S5)}$$

$$where,\ G(J) = \frac{dV}{d(\ln J)},\ H(J) = V - \frac{\eta k_B T}{q_e} \ln\left(\frac{J}{A^* T^2}\right)$$

The ideality factor (η) which is a measure of the diode to be ideal for pure thermionic emission,[14] was determined from the intersection of the y-axis for the linear region of the equation (S4) (Fig. S9). The barrier height (ϕ_B) was estimated from the intersection of the equation (S5). The series resistance (R_S) was found both from equation (S4) and (S5) and the values of resistances are enlisted in Table-3 (main article) along with values of ideality factor and barrier height.

SCLC parameters:

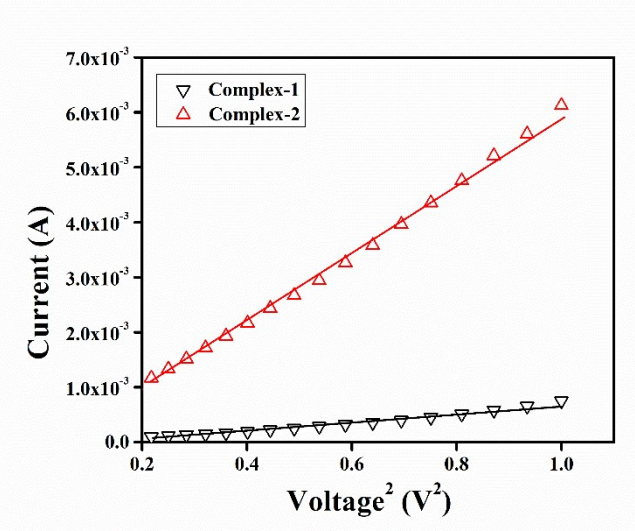

Figure S6: I vs. V^2 plot for complexes **1** and **2**.

References

1 M. A. Spackman and D. Jayatilaka, *CrystEngComm,* 2009, **11**, 19-32.

2 F. L. Hirshfeld, *Theor. Chim. Acta,* 1977, **44**, 129-138.

3 A. L. Rohl, M. Moret, W. Kaminsky, K. Claborn, J. J. McKinnon and B. Kahr, *Cryst. Growth Des.*, 2008, **8**, 4517-4525.

4 A. Parkin, G. Barr, W. Dong, C. J. Gilmore, D. Jayatilaka, J. J. McKinnon, M. A. Spackman and C. C. Wilson, *CrystEngComm*, 2007, **9**, 648-652.

5 M. A. Spackman and J. J. McKinnon, *CrystEngComm*, 2002, **4**, 378-392.

6 S. K. Wolff, D. J. Grimwood, J. J. McKinnon, D Jayatilaka, M. A. Spackman, Crystal Explorer 2.0; University of Western Australia: Perth, Australia, 2007. http://hirshfeldsurfacenet.blogspot.com/.

7 F. H. Allen, O. Kennard, D. G. Watson, L. Brammer, A. G. Orpen and R. J. Taylor, *J. Chem. Soc. Perkin Trans.2*, 1987, S1-S19.

8 J. J. Kinnon, M. A. Spackman, A. S. Mitchell, *Acta Cryst.*, 2004, **B60**, 627-668.

9 S. Emamian, T. Lu, H. Kruse and H. Emamian, J. Comput. Chem., 2019, **40**, 2868–2881.

10 O. Kahn, Molecular magnetism, VCH, New York, 1993.

11 J. Tauc, *Amorphous and Liquid Semiconductors, Plenum Press*, New York, 1974.

12 R. Jana, A. Dey, M. Das, J. Datta, P. Das, P. P. Ray, *Applied Surface Science,* 2018, **452**, 155–164

13 K. Cheung, N. W. Cheung, *Appl. Phys. Lett.,* 1986, **49**, 85-87

14 M. Sahina, H. Safaka, N. Tugluoglub and S. Karadeniz, *Applied Surface Science* 2005, **242**, 412–418.